

Next-Frame Decoding for Ultra-Low-Bitrate Image Compression with Video Diffusion Priors

Yunuo Chen¹ Chuqin Zhou¹ Jiangchuan Li¹ Xiaoyue Ling¹ Bing He¹

Jincheng Dai² Li Song¹ Guo Lu^{1*}

¹Shanghai Jiao Tong University

²Beijing University of Posts and Telecommunications

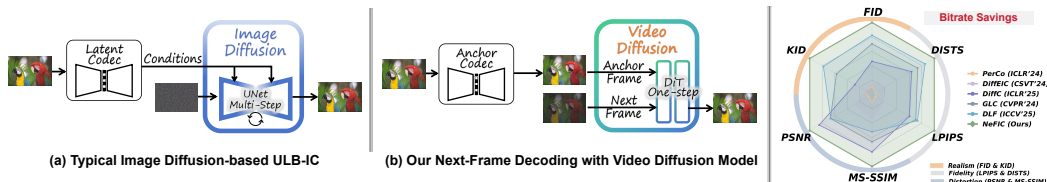


Figure 1: (a) Some previous diffusion-based ULB-IC methods transmit latents that serve as conditions for image diffusion models during generative decoding. (b) Our method decodes a compact anchor frame and uses a video diffusion model to evolve this anchor into the target image via next-frame prediction. Radar plot compares our model with recent generative codecs on the CLIC2020 test set.

Abstract

We present a novel paradigm for ultra-low-bitrate image compression (ULB-IC) that exploits the “temporal” evolution in generative image compression. Specifically, we define an explicit intermediate state during decoding: a compact anchor frame, which preserves the scene geometry and semantic layout while discarding high-frequency details. We then reinterpret generative decoding as a virtual temporal transition from this anchor to the final reconstructed image. To model this progression, we leverage a pretrained video diffusion model (VDM) as temporal priors: the anchor frame serves as the initial frame and the original image as the target frame, transforming the decoding process into a next-frame prediction task. In contrast to image diffusion-based ULB-IC models, our decoding proceeds from a visible, semantically faithful anchor, which improves both fidelity and realism for perceptual image compression. Extensive experiments demonstrate that our method achieves superior objective and subjective performance. On the CLIC2020 test set, our method achieves over **50% bitrate savings** across LPIPS, DISTs, FID, and KID compared to DiffC, while also delivering a significant decoding speedup of up to $\times 5$. Code will be released later.

1 Introduction

The explosive growth of image data has sharply increased storage and transmission burdens, motivating steady progress in high-performance lossy image compression. Learned image compression (LIC) has advanced rapidly under variational autoencoders (VAEs) and end-to-end optimization [1, 2]. Early models relied on CNN-based analysis-synthesis transforms [3, 4, 5], while later Transformer- and Mamba-based architectures further improved the rate-distortion (RD) performance [6, 7, 8, 9, 10, 11, 12, 13, 14, 15, 16, 17, 18, 19, 20]. Concurrently, the rise of Generative Adversarial Network (GAN) [21] and diffusion models [22, 23] has reframed ultra-low-bitrate image compression as a pivotal frontier. By leveraging powerful generative priors, diffusion-based codecs can deliver

*Corresponding Author

striking perceptual realism at extremely low bitrates. Most existing approaches [24, 25, 26] control the multi-step denoising process via controlling networks (Fig.1 (a)). However, the unclear influence of the conditional signals on diffusion process and the uncertainty of Gaussian initialization potentially induce semantic drift and weaken faithfulness to the source [27, 24, 28, 29]. In addition, the iterative denoising process incurs substantially higher computational cost and decoding latency than conventional VAE-style codecs. So far, the central challenge for ULB-IC is to achieve simultaneously: (i) strong perceptual realism, (ii) source-content faithfulness, and (iii) practical inference efficiency.

To achieve these targets, we propose a novel paradigm for ultra-low-bitrate image compression that explores the dynamics in generative image decoding. Instead of treating image reconstruction as a static process, our framework reinterprets single-image generative decoding as a virtual temporal process, where a compact anchor evolves to a high-fidelity reconstructed image.

We define an explicit intermediate state for ULB-IC: a visible anchor that preserves scene geometry, semantic layout, and coarse appearance while discarding high-frequency details. As shown in Fig. 1 (b), this anchor is encoded by a VAE-based Anchor Codec. At the decoder, we first decode the anchor from the bitstream and treat it as the initial state. The evolution from anchor to fine-grained reconstruction is then modeled as a video-like progression using a VDM. We construct a virtual two-frame video, where the anchor is the first frame and the original image is the second. This setup casts generative decoding as a next-frame prediction task conditioned on the anchor, guided by the dynamic priors of the VDM. This yields a reconstruction consistent with the anchor and perceptually aligned with the source without extra control networks, improving both realism and fidelity.

However, two key challenges arise when applying video diffusion models to image compression. (1) **Domain Gap Between Video Generation and Image Decoding.** Video diffusion models are primarily trained for gradual temporal evolution across dozens of frames, and emphasize scene transitions and object motions. In contrast, our goal is to achieve high-fidelity detail synthesis through a single-interval transition: a virtual two-frame “video” consisting solely of the compact anchor and the target image. (2) **High Computational Cost of Iterative Denoising.** State-of-the-art VDMs often require 50 iterative denoising steps and start from standard Gaussian noise, causing high latency and injecting ambiguity that can harm fidelity [24, 27]. Our aim is to turn multi-step video diffusion into a *one-step* generative decoder that preserves both fidelity and realism.

To address these challenges, we propose a two-stage training scheme that adapts VDMs for efficient and faithful ultra-low-bitrate image decoding: **Stage I: Next-Frame Decoding Adaptation.** We jointly finetune the pretrained VDM and the anchor codec to synthesize high-fidelity details from compact anchor frames while suppressing undesirable temporal artifacts, such as object motion and scene flicker. This adaptation aligns the generative priors of the VDM with the anchor-conditioned detail synthesis process, enabling accurate and perceptually faithful reconstruction through a single-step temporal evolution. **Stage II: One-Step Generative Bypass.** To eliminate the latency introduced by iterative denoising, we collapse the multi-step diffusion process to one-step generation by establishing a latent bypass between anchor compression and video generation. Specifically, we condition the encoding of the anchor Compression-VAE on generative latents obtained from the Video-VAE. We then introduce a Bypass Refinement module, which is a learned mapping from the compression latent space to the generative latent space. This bypass regularizes and aligns the latent spaces of the two VAEs, reducing generative uncertainty and enabling faithful one-step decoding.

Our contributions can be summarized as follows.

1. **A novel ULB-IC paradigm:** We reinterpret generative image decoding as a virtual temporal transition from a compact anchor into a faithful realistic reconstruction.
2. **Efficient generative decoding:** Our two-stage training pipeline adapts VDMs for compression-aware next-frame prediction while enabling one-step generation.
3. **State-of-the-art performance:** Extensive experiments demonstrate that our model achieves superior perceptual realism and fidelity with relatively faster decoding.

2 Related Work

2.1 Generative Image Compression

VAE- and GAN-based Codecs. Previous VAE-based learned image compression models [30, 4, 31, 32, 33, 3, 34, 35, 36] mainly optimize standard objective metrics, such as PSNR and MS-SSIM.

Agustsson *et al.* [37] and HiFiC [38] start GAN-based methods for low bitrate image compression and aim to improve realism and fidelity. MR [39] connects generative and non-generative compression. MS-ILLM [40] introduces a local likelihood model to improve realism. EGIC [41] uses discriminators conditioned on segmentation. Recent studies [42, 43, 44] use vector quantization for extreme semantic compression. TACO [45] proposes a text-guided encoder to improve fidelity.

Diffusion-based Codecs. Recent works [46, 47, 48, 49, 50, 51, 52, 53, 54, 55, 56, 57, 29, 58, 59, 60, 61, 62, 63, 64] use generative priors from large pretrained controllable image diffusion models [65, 66, 67]. Building on DDPM [23] and LDM [68], they show better perceptual realism than GAN-based methods. [24] introduces a privileged decoder to correct the denoising process. DiffC [69] achieves zero-shot compression using reverse-channel coding. ResULIC [28] adds residual coding for semantic alignment. PICD [61] proposes a generative codec for both screen contents and natural images. Most models [70, 71, 25, 72] based on standard image diffusion models mainly inject conditions through channel concatenation, which may not be a principled way to exploit context.

2.2 Video Diffusion Model

The evolution of text-to-video (T2V) synthesis has been fast and significant. Early work with large-scale Transformers, such as CogVideo [73] and Phenaki [74], showed that the approach was feasible with great potential. Later advanced diffusion models [75, 76, 77, 78, 79] brought a clear jump in generation quality. With the development in the Diffusion Transformer (DiT) architecture, LinGen [80], CogVideoX [81] and OpenAI’s Sora [82] reached a new level for text-to-video generation. Recently, WAN [83], Tencent’s Hunyuan-DiT [84] and OpenAI’s Sora-2 [85] together mark the current frontier of modern video generation.

3 Methodology

3.1 Preliminary: In-Context Learning in VDMs.

We build upon CogVideoX-1.5 [81], a text-to-video diffusion model that generates frame sequences by progressively denoising latent noise conditioned on a text prompt. The architecture comprises: (1) a 3D causal Video-VAE for joint spatio-temporal compression whose encoder maps input videos to latents at 1/8 height and width; (2) a text encoder [86] producing prompt embeddings; and (3) a DiT-based [87] noise-prediction transformer. The transformer operates on the concatenation of text and video tokens with 3D attention and applies 3D rotary position embeddings [88] to queries and keys for spatial-temporal modeling.

As a video foundation model trained on large-scale continuous visual data, CogVideoX exhibits emergent behaviors analogous to LLMs, including unified generation and in-context learning [89, 90]. Given preceding frames $\{c_1, c_2, \dots\}$ as context, it autoregressively predicts subsequent frames $\{y_1, y_2, \dots\}$ by capturing long-range spatio-temporal dependencies. This next-token-style formulation supports continued pretraining and task-specific finetuning, enabling coherent future-frame synthesis that remains consistent with the provided visual context.

3.2 Reframing Generative Image Compression

As discussed in Sec. 1, we focus on modeling the transition from a compact anchor to a high-fidelity reconstruction with video diffusion priors. We adopt a two-frame abstraction: the anchor image serves as the first frame for video generation, and the target reconstruction as the second. Accordingly, we reinterpret the anchor as the conditional frame and task the VDM to predict the next frame that restores realistic details. As shown in Fig. 2, the encoding and generative decoding process for image x can be defined as

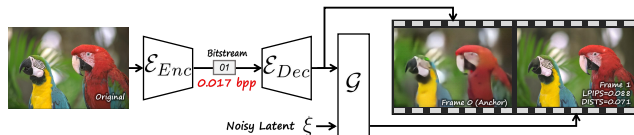


Figure 2: An illustration of our next-frame prediction paradigm for generative codec.

As shown in Fig. 2, the encoding and generative decoding process for image x can be defined as

$$\hat{x} = (\mathcal{G} \circ \mathcal{E}_{Dec})(l; \xi), \quad l = Q(\mathcal{E}_{Enc}(x)), \quad (1)$$

where \mathcal{E}_{Enc} is the encoder of the Anchor Codec and Q denotes quantization. ξ represents the noisy latent input of the target frame and l refers to the transmitted latent. \mathcal{E}_{Dec} denotes the anchor decoder, and \mathcal{G} is a VDM adapted for single-interval photorealistic next-frame prediction.

In the following sections, we introduce our two-stage training scheme designed to bridge the domain gap between video generation and image decoding, and to mitigate the computational overhead of multi-step diffusion sampling. These stages together enable efficient and faithful image decoding within our generative compression framework.

3.3 Why is a VDM preferred over an image diffusion model (IDM)?

1. Temporal Prior: VDM’s built-in transition capability.

Our key insight is that pretrained VDMs can naturally generate **temporal defocus-to-focus transitions**: starting from vague frames, VDMs generate high-frequency details in the subsequent frames. As shown in Fig. 3, details of parrot feathers are temporally refined.

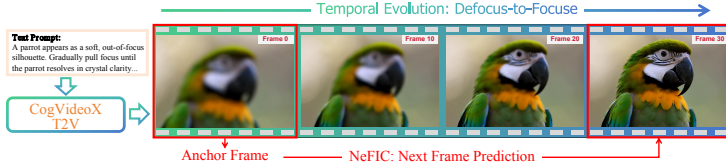


Figure 3: **Defocus-to-Focus Temporal Transition Prior.** These generated frames show that VDM generates natural textures where appropriate (e.g., parrot feathers). NeFIC exploits this property and collapses multi-frame transitions into next-frame prediction.

This behavior is not incidental. Trained on large-scale video data, VDMs internalize world knowledge and inter-object relations. Since video corpora contain abundant “defocus-to-focus” temporal patterns, VDMs learn to temporally refine coarse structure into detail-resolved imagery.

We repurpose this generative prior: heavily compressed anchors represent the early blurry frames, while the final reconstructions correspond to the clear frames at the end. This is significantly different from predicting residuals [70, 71]. **NeFIC reinterprets the blur-to-clarity temporal transition (rather than motion) in VDM as generative decoding. This pretrained transition prior is not internalized by IDMs.**

2. Architectural Advantages: Leveraging VDM’s 3D spatiotemporal structure and in-context learning capability.

Inspired by in-context learning in LLMs, we reformulate VDM-based generative decoding as conditional next-frame prediction. We fully exploit the pretrained **3D Attention** and **3D RoPE**: NeFIC performs frame/token-level concatenation to treat the anchor frame as a preceding context.

IDM-based codecs typically inject conditions by concatenating the conditional latent with the noisy latent along the channel dimension [70, 71, 25, 72]. Thus, conditional interactions occur only through implicit cross-channel feature mixing. By contrast, token concatenation coupled with 3D Attention enables explicit and adaptive retrieval: each noisy token can directly attend to and query any anchor token. Meanwhile, 3D RoPE imposes a correspondence prior along the temporal axis, biasing attention toward spatially aligned regions across frames. Thus, NeFIC synthesizes high-frequency details as structurally anchored refinements of the coarse layout. **NeFIC inherits VDM’s 3D inductive bias as a more principled condition-injection pathway. This effective conditional generation and in-context learning capabilities are not supported by standard IDMs.**

3.4 Stage I: Next-Frame Decoding Adaptation

We first cast generative decoding as a single-interval next-frame prediction in the latent space of a frozen Video-VAE. This stage focuses on synthesizing fine-grained details while suppressing undesirable temporal artifacts, such as object motions and scene flicker. During training, we adapt the DiT [87] blocks to condition on the decoded anchor, and to predict the clean latent of the target frame from its noised latent at diffusion step $t \in \{1, \dots, T\}$ with schedule (α_t, σ_t) satisfying $\alpha_t^2 + \sigma_t^2 = 1$. For efficiency, we finetune only the Anchor Codec and the attention projections (W_q, W_k, W_v, W_{out}) via LoRA [91], while keeping the Video-VAE and the text encoder frozen. The video diffusion priors provide photorealistic texture and detail synthesis without auxiliary control networks.

Tokenization and Conditioning. Let E_{text} denote the frozen text encoder, E_{vid} the frozen Video-VAE encoder, f_θ the DiT blocks, and \oplus token-sequence concatenation. The model consumes three sequences of tokens:

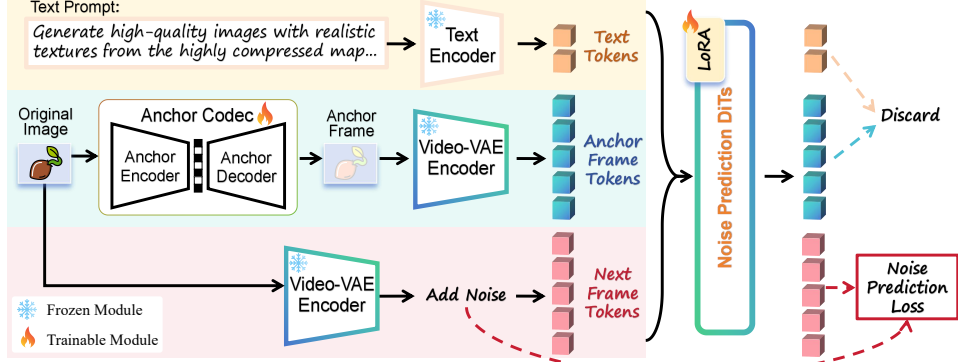


Figure 4: **Overview of Training Stage I.** The input to the DiT blocks is a concatenation of three types of tokens: (1) text embeddings, (2) tokens from the anchor frame, and (3) noised tokens from the target frame. During training, only the output corresponding to the noised target tokens is supervised using a noise prediction loss, while the other two segments are discarded.

1. **Text tokens:** $\mathbf{z}_{\text{text}} = E_{\text{text}}(p)$, where p is a universal prompt (“generate a high-quality image with realistic texture...”). Our framework eliminates the need for detailed scene descriptions, as conditions and semantics are fully transmitted via anchor frames. The text prompt serves only as a guidance of the transition behavior.
2. **Anchor tokens:** $\mathbf{z}_{\text{anchor}} = E_{\text{vid}}(\mathcal{E}_{\text{Dec}}(l))$, obtained by encoding the decoded anchor $\mathcal{E}_{\text{Dec}}(l)$, which serves as the initial-frame condition.
3. **Noisy target tokens:** \mathbf{z}_t , formed by encoding the original image x into $\mathbf{z}_0 = E_{\text{vid}}(x)$ and adding noise:

$$\mathbf{z}_t = \alpha_t \mathbf{z}_0 + \sigma_t \epsilon, \quad \epsilon \sim \mathcal{N}(\mathbf{0}, \mathbf{I}). \quad (2)$$

Noise Prediction and Loss. We condition on $\mathbf{c} = \mathbf{z}_{\text{text}} \oplus \mathbf{z}_{\text{anchor}}$ and feed $\mathbf{c} \oplus \mathbf{z}_t$ into f_θ at step t . Using v -prediction parameterization [92], we reconstruct target latent as

$$\mathbf{v}_\theta^{(t)}(\mathbf{z}_t, \mathbf{c}) = f_\theta(\mathbf{z}_t, \mathbf{c}, t), \quad (3)$$

$$\hat{\mathbf{z}}_0 = \alpha_t \mathbf{z}_t - \sigma_t \mathbf{v}_\theta^{(t)}(\mathbf{z}_t, \mathbf{c}) \quad (4)$$

The output tokens corresponding to the text and anchor segments are discarded. Only the output token segment aligned with the target tokens is supervised as

$$\mathcal{L}_{\text{noise}} = \|\hat{\mathbf{z}}_0 - \mathbf{z}_0\|_2^2. \quad (5)$$

Auxiliary Anchor Loss. To keep the decoded anchor $x_{\text{anchor}} = \mathcal{E}_{\text{Dec}}(l)$ within the training distribution of the Video-VAE and maintain its conditioning strength, we add an auxiliary reconstruction term on x_{anchor} :

$$\begin{aligned} \mathcal{L}_{\text{aux}} = & \lambda_{\text{MSE}} \|x - x_{\text{anchor}}\|_2^2 \\ & + \lambda_{\text{LPIPS}} \text{LPIPS}(x, x_{\text{anchor}}), \end{aligned} \quad (6)$$

with $\lambda_{\text{MSE}} = 5$ and $\lambda_{\text{LPIPS}} = 1$. The MSE term enforces pixel-level fidelity so the anchor remains stably encodable by E_{vid} ; the LPIPS term [93] preserves perceptual similarity and high-level semantics, ensuring sufficient and faithful semantic information for conditioning.

Overall Objective. The Stage I objective combines noise prediction, anchor regularization, and a bitrate penalty:

$$\mathcal{L}_{\text{stageI}} = \mathcal{L}_{\text{noise}} + \lambda_{\text{aux}} \mathcal{L}_{\text{aux}} + \lambda_R R, \quad (7)$$

where R is the bitrate loss of the anchor frame and λ_R trades rate against reconstruction quality.

This stage encourages VDM LoRAs to learn the conditional dependence in the compact anchor $\mathbf{z}_{\text{anchor}}$, thereby modeling the next-frame transition and recovering a fine-grained latent $\hat{\mathbf{z}}_0$ under multi-step diffusion.

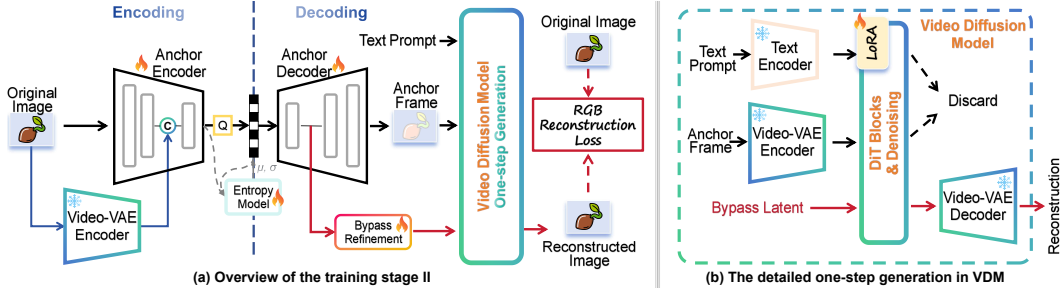


Figure 5: **Overview of Training Stage II. (a) Compression & decompression.** The Anchor Encoder is conditioned on Video-VAE latents of the original image and produces entropy-coded anchor latents. The Anchor Decoder reconstructs the anchor frame, and a bypass latent is generated from the decoding process. **(b) Detailed One-step generation.** A single-step video diffusion model consumes text embeddings, anchor tokens, and the bypass latent to predict the target latent, which the Video-VAE decoder converts to final reconstruction.

3.5 Stage II: One-Step Generative Bypass

To collapse multi-step denoising into a single step, we initialize target latent with an informative latent instead of Gaussian noise, which helps to reduce ambiguity and semantic drifts [27]. Concretely, we introduce a latent bypass that couples the Anchor Codec to the video diffusion generator, implemented through the two strategies detailed below.

Conditional Anchor Encoding. Due to the latent-space gap between the compression-VAE and generative-VAE [94], raw features of the anchor codec are suboptimal for diffusion. Inspired by conditional coding [5, 95, 96], we condition and align the anchor encoder with the Video-VAE-encoded latents. The frozen E_{Vid} encodes the original image x to a 1/8-scale latent $\mathbf{z}_0 = E_{\text{Vid}}(x)$. As shown in Fig. 5, at the same spatial scale the Anchor encoder produces a feature map \mathbf{h}_{enc} . We concatenate them along channels $\mathbf{h}_{\text{cond}} = [\mathbf{h}_{\text{enc}}; \mathbf{z}_0]$, then apply the codec transforms, entropy modeling, and quantization to \mathbf{h}_{cond} . This biases the Anchor Codec to preserve more scene information and layout semantics consistent with the diffusion prior. As shown in Fig. 6, removing the conditional encoding for the anchor (“w/o Cond-Enc”) leads to semantic drift, such as the appearance of extra teeth in the mouth.

Bypass Refinement. We decode a bypass latent from the anchor decoding path to replace stochastic noise at inference. Let \mathbf{h}_{dec} be the 1/8-scale feature from \mathcal{E}_{Dec} . A Transformer-based Semantic Bypass Refinement T maps $\mathbf{z}_{\text{bypass}} = T(\mathbf{h}_{\text{dec}})$, which serves as the initial noisy latent



Figure 6: Reconstruction visualizations of three variants.

for one-step generation, carrying semantics aligned to the generation manifold. We also provide comparison results in Fig. 6, where the absence of bypass refinement causes semantic information to become ambiguous and the reconstruction of teeth to appear vague. This occurs because the increasing gap between the compression and generation latent spaces exacerbates the denoising difficulty for DiTs.

One-step generation. As in Stage I, we form $\mathbf{c} = \mathbf{z}_{\text{text}} \oplus \mathbf{z}_{\text{anchor}}$, where $\mathbf{z}_{\text{text}} = E_{\text{text}}(p)$ and $\mathbf{z}_{\text{anchor}} = E_{\text{VidE}}(x_{\text{anchor}})$. To enable one-step generation, we model the bypass latent as a partially denoised state and set the denoising step t^* to half of the maximum step value, specifically 500. Using v -prediction, the DiT predicts noise and reconstructs the clean latent in a single step

$$\mathbf{v}_{\theta}(\mathbf{z}_{\text{bypass}}, \mathbf{c}, t^*) = f_{\theta}(\mathbf{z}_{\text{bypass}}, \mathbf{c}, t^*), \quad (8)$$

$$\hat{\mathbf{z}}_0 = \alpha_{t^*} \mathbf{z}_{\text{bypass}} - \sigma_{t^*} \mathbf{v}_{\theta}(\mathbf{z}_{\text{bypass}}, \mathbf{c}, t^*), \quad (9)$$

where $(\alpha_{t^*}, \sigma_{t^*})$ is the fixed one-step schedule. The frozen Video-VAE decoder yields $\hat{x} = D_{\text{Vid}}(\hat{\mathbf{z}}_0)$.

CLIP-based GAN loss. To leverage semantic priors from visual foundation models, we adopt a CLIP-based [97] discriminator for adversarial training. Following [98], we train a lightweight

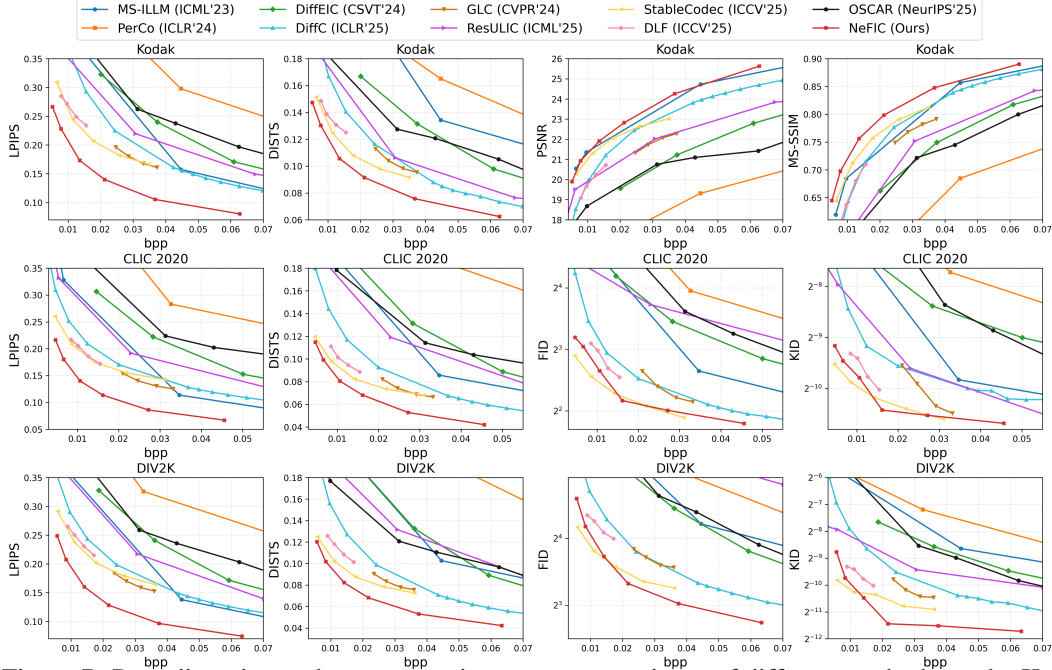


Figure 7: Rate-distortion and rate-perception curve comparisons of different methods on the Kodak, CLIC 2020 and DIV2K dataset.

classifier head on top while keeping the CLIP backbone frozen. The adversarial loss \mathcal{L}_{GAN} helps narrow the distribution gap between x and \hat{x} [94, 38].

RGB reconstruction loss. The reconstruction loss combines the GAN term with pixelwise and perceptual criteria:

$$\begin{aligned} \mathcal{L}_{RGB} = & \lambda_{GAN} \mathcal{L}_{GAN} + \lambda_{MSE} \|\hat{x} - x\|_2^2 \\ & + \lambda_{LPIPS} \text{LPIPS}(\hat{x}, x), \end{aligned} \quad (10)$$

with $\lambda_{GAN} = 1$, $\lambda_{MSE} = 2.5$, $\lambda_{LPIPS} = 0.5$.

Overall objective. We retain the auxiliary anchor loss \mathcal{L}_{aux} and the bitrate loss R from entropy model as Stage I. The Stage II overall training objective is defined as

$$\mathcal{L}_{stageII} = \mathcal{L}_{RGB} + \lambda_{aux} \mathcal{L}_{aux} + \lambda_R R, \quad (11)$$

In Stage II, we update parameters of bypass refinement module T , the Anchor Codec (i.e., \mathcal{E}_{Enc} , \mathcal{E}_{Dec}), and the LoRA adapters of f_θ . Other parts remain frozen.

4 Experiments

4.1 Model and Training.

Experimental Settings. We use CogVideo-X1.5 as the video diffusion backbone for our model and pretrain a VAE-based Anchor Codec. Details are in the supplementary material. Our models are trained on Flickr2W [99] with random square crops whose side length is uniformly sampled from 512 to 768 pixels. We set the batch size to 8 and train for 10k steps for stage I and 50k steps for stage II. In stage I, the learning rate is $1e-4$. In stage II, we introduce the CLIP-based GAN loss at 35k steps and decay the learning rate to $1e-5$ at 45k steps. The whole 2-stage training takes about 3 days. All models are optimized with AdamW. λ_{aux} is fixed at 0.1, λ_R is chosen from $\{5, 3, 1.7, 1.0, 0.5, 0.25\}$.

Evaluation. We evaluate all the methods on Kodak [100], the CLIC2020 test set [101], and DIV2K [102]. We report objective distortion (PSNR, MS-SSIM), perceptual fidelity metrics (LPIPS [93], DISTs[103]), and perceptual realism metrics (FID [104], KID [105]). Bit-rate efficiency is measured using Bjøntegaard-Delta rate (BD-rate) [106]. We compute PSNR/MS-SSIM/LPIPS/DISTs on full-resolution images. Following HiFiC [38], FID and KID are computed on 256×256 patches for

Model	Kodak				DIV2K				CLIC2020 Test			
	LPIPS	DISTS	PSNR	MS-SSIM	LPIPS	DISTS	FID	KID	LPIPS	DISTS	FID	KID
MS-ILLM [40]	10.76	203.21	-32.27	-19.59	35.40	104.69	143.45	173.20	28.71	75.29	94.68	747.20
PerCo [25]	112.61	202.54	303.82	146.77	266.60	409.65	176.61	170.99	326.11	452.83	128.88	54.05
DiffEIC [26]	61.15	84.54	121.28	77.12	106.71	134.88	162.47	141.98	131.51	158.89	73.68	38.45
GLC [44]	-16.86	-6.07	55.25	27.76	-17.79	-15.28	3.25	-21.90	-18.12	-18.72	-32.22	-36.10
DiffC [69]	0.00	0.00	0.00	0.00	0.00	0.00	0.00	0.00	0.00	0.00	0.00	0.00
ResULIC [28]	-9.28	-6.83	7.60	24.38	38.02	68.73	269.67	0.57	42.08	64.07	32.80	-62.06
StableC [94]	-42.19	-41.20	-22.05	-20.82	-27.31	-47.56	-52.06	-70.08	-27.39	-48.35	-70.67	-73.46
DLF [29]	-42.31	-36.97	7.77	-1.25	-20.07	-33.97	-25.71	-34.37	-22.51	-36.44	-60.82	-67.93
OneDC [55]	-44.31	-28.60	12.47	0.37	-48.51	-36.90	-36.12	-	-54.55	-46.49	-43.06	-
OSCAR [62]	35.16	28.74	95.69	51.56	143.25	43.65	171.66	-	196.58	97.54	352.81	-
NeFIC(Ours)	-64.03	-50.84	-34.26	-33.88	-61.71	-56.94	-49.94	-71.20	-64.09	-57.96	-65.76	-75.94

Table 1: Detailed BD-Rate of different ultra-low-bitrate image compression models on Kodak, DIV2K and CLIC2020 test set.

CLIC2020 and DIV2K. We omit FID/KID on Kodak because its small size (24 images) precludes reliable distribution estimation.

Baselines. We take generative image codecs as baselines, including the VAE- and GAN-based generative codec MS-ILLM[40], GLC[44], DLF[29] and recent diffusion-based methods: PerCo[25], DiffEIC[26], DiffC[69], ResULIC[28], OSCAR[62], OneDC[55] and StableCodec [94].

4.2 Main Results

4.2.1 Quantitative Evaluation

Perceptual Metrics. In Fig. 7, we plot rate-perception curves across various datasets. The corresponding BD-rate results are summarized in Tab. 1 (lower is better; negative indicates bitrate savings), where we report BD-Rate on DIV2K with DiffC as the baseline. Compared with the earlier diffusion-based codec PerCo [25], our model reduces bitrate on DIV2K by 89.82%, 91.61%, 87.94%, and 93.25% on LPIPS, DISTS, FID, and KID, respectively. Even against recent SOTA method DLF [29] (ICCV’2025), our method still achieves 51.92%, 48.16%, 31.82%, and 33.47% BD-rate savings on the same four metrics. Across datasets and metrics, our approach consistently attains substantial bitrate reductions at matched perceptual quality, indicating that it preserves both perceptual realism and image fidelity.

Distortion Metrics. Tab. 1 also reports BD-rate comparisons on PSNR and MS-SSIM for Kodak; the corresponding RD curves are shown in Fig. 7. Whereas many generative compression methods sacrifice distortion-oriented objectives for stronger generative ability, our method improves both perceptual and distortion metrics. On Kodak, we outperform recent SOTA model StableCodec [94] (ICCV’2025) by 18.27% BD-rate on PSNR and 22.95% on MS-SSIM. Compared to GAN-based method GLC [44] (CVPR’24), our model can also achieve 57.08% and 46.91% bitrate savings for PSNR and MS-SSIM. These advantages in objective metrics attest to the faithfulness of our reconstructions. Detailed PSNR and MS-SSIM results for DIV2K and CLIC2020 are provided in the supplementary.

The consistent gains in realism, fidelity, and distortion metrics stem from our evolutionary decoding. The anchor frame preserves coarse yet faithful structure and key semantics, while the video diffusion prior, with its strong temporal consistency, refines them into realistic fine textures. This yields a tight latent-pixel dual-domain coupling: the bypass latent provides a good initialization in latent space, and the anchor frame offers a pixel-domain reference that fully exploits the pretrained video consistency.

4.2.2 Qualitative Evaluation.

We present qualitative comparisons of our NeFIC, our anchor frame, and previous diffusion-based ULB-IC models in Fig. 8. At ultra-low bit rates, NeFIC produces details that are more visually consistent with and faithful to the original image. For instance, our model accurately reconstructs the regular ridges on glassware, as well as irregular corrosion patterns on walls. Other models fail to recover those details accurately. Despite using higher bitrates than our approach, these competing models perform worse for LPIPS, DISTS, and visual fidelity. As we described, our anchor frame



Figure 8: Qualitative examples on the CLIC2020 dataset. Zoom in for better view. More comparisons are in supplementary.

Model	Kodak (s)		DIV2K (s)		BD-Rate DIV2K (LPIPS,%)
	Enc.	Dec.	Enc.	Dec.	
PerCo [25]	0.39	1.92	0.62	38.29	266.60
DiffEIC [26]	0.23	4.82	2.42	58.46	106.71
DiffC [69]	0.6–9.1	2.9–8.4	3.4–47.2	15.8–37.7	0.00
StableCodec [94]	0.11	0.14	18.86	40.63	-27.31
w/o Stage II	0.16	30.61	0.51	296.02	-47.01
NeFIC (Ours)	0.17	0.88	0.58	6.83	-61.71

Table 2: Runtime (s) on Kodak and DIV2K.

Model variants	LPIPS	DISTS	FID	KID
w/o Stage I	-52.32	-44.71	-40.32	-62.88
w/o Stage II	-47.01	-42.03	-53.72	-77.91
w/o Conditional Encoding	-56.81	-52.34	-42.01	-62.46
w/o Bypass Refinement	-48.01	-47.19	-39.36	-57.91
w/o Aux Anchor Loss	-19.78	-20.46	-31.07	-40.74
w/o CLIP-based GAN	-63.09	-64.02	-30.31	-30.07
NeFIC (Ours)	-61.71	-56.94	-49.94	-71.20

Table 3: Ablation BD-rate results.

preserves only the scene geometry, semantic layout, and coarse appearance, while providing a powerful temporal initialization for next-frame decoding.

4.3 Efficiency Evaluation.

We assess runtime efficiency as the average per-image encoding (Enc.) and decoding (Dec.) time on an A100 GPU on the Kodak and DIV2K datasets (Tab. 2). NeFIC achieves 0.17/0.88 s (Enc./Dec.) on Kodak and 0.58/6.83 s on DIV2K, yielding 5.5-8.6 \times faster decoding and 1.35-4.17 \times faster encoding than the diffusion-based DiffEIC. On high-resolution DIV2K, NeFIC outperforms StableCodec by 32.5 \times in encoding and 6.0 \times in decoding due to avoiding costly tiling. These gains arise from single-interval prediction and one-step generation, which yield smoothly scaling latency and avoid the sharp slowdowns of multi-step diffusion or heavy tiling. Removing the second stage training for one-step generation increases decoding time to 30.61s for Kodak and 296.02s for DIV2K in a 50-step denoising setting. These delays are unacceptable and underscore the effectiveness and necessity of our generative bypass.

4.4 Ablation Studies.

We ablate the key design components of NeFIC. Unless otherwise noted, all variants are evaluated on DIV2K using LPIPS, DISTS, FID, and KID, with DiffC as the baseline.

Stage I (Next-Frame Adaptation). Training directly with Stage II is possible but suboptimal. CogVideoX is pretrained on long video sequences (> 25 frames) with diverse scene transitions and motions [81]. If we skip Stage I, the LoRA must learn compression-aware single-interval prediction and single-step generation at the same time, which makes optimization harder and more unstable. In Tab. 3, removing Stage I (“w/o Interval Adaptation”) degrades BD-Rate on all four metrics by 8-10%.

Stage II (One-step Bypass). With Stage I alone, the model supports next-frame decoding for ultra-low bitrate compression but still requires multi-step denoising. Adding Stage II enables end-to-end training and further improves fidelity, at the cost of slightly lower realism. Compared with the Stage I-only setting (“w/o One-step Bypass”), Stage II improves LPIPS and DISTS BD-Rate by about 15%, while FID and KID worsen by roughly 4% and 7%, indicating a mild trade-off between perceptual fidelity and realism.

Generation Model	LPIPS	DISTS	FID	KID
(1) FLUX-12B (w/o anchor)	-32.01	-33.21	-53.97	-72.87
(2) FLUX-12B (channel concatenation)	-35.77	-35.13	-55.92	-72.09
(3) FLUX-12B (token concatenation)	-42.18	-42.31	-53.98	-73.19
CogVideoX-5B (Ours)	-61.71	-56.94	-49.94	-71.20

Table 4: Paradigm and Foundation Model Comparison.

LoRA Rank/Alpha	LPIPS	DISTS	FID	KID
64/64	-44.18	-41.01	-59.91	-82.99
128/128	-54.82	-51.36	-58.34	-80.26
256/256	-61.71	-56.94	-49.94	-71.20

Table 5: Ablations on LoRA Configuration.

Conditional Encoding. The semantic latent bypass consists of *Conditional Encoding* and *Bypass Refinement*. Removing Conditional Encoding hampers the alignment of the bypass latent with the VDM generation space and its cooperation with the frozen Video-VAE decoding, yielding BD-rate drops about 4.9% for LPIPS and 7.9% for FID (Tab. 3).

Bypass Refinement. Ablating the transformer-based bypass refinement causes a larger gap: BD-Rate degrades by $\sim 10\text{-}14\%$ on LPIPS/FID/KID. This suggests the raw VAE-decoded latent still mainly supports anchor-frame RGB reconstruction, while refinement better adapts it to the VDM generation space with stronger semantics.

Auxiliary Anchor Loss. Without the auxiliary anchor loss, the anchor frame diverges from the natural image domain, exhibiting significant semantic and color drift. This misalignment with the training distribution of Video-VAE weakens the conditioning for next-frame generation for single-interval, one-step decoding. In Tab. 3, the absence of this loss leads to a substantial degradation in perceptual compression performance, with BD-Rate degrading to -19.78% for LPIPS and -40.74% for KID.

CLIP-guided GAN Loss. Ablating the CLIP-based adversarial loss slightly improves LPIPS/DISTS but severely harms realism (FID/KID worsen by about 20 and 41 BD-Rate points). Adversarial training is therefore important for preserving generation capability and generative realism.

LoRA Settings. Tab. 5 shows that increasing rank/alpha from 64/64 to 256/256 consistently improves LPIPS ($-44.18\% \rightarrow -61.71\%$) and DISTS ($-41.01\% \rightarrow -56.94\%$) while degrading FID and KID by about 10% in BD-rate. We adopt 256/256 as the default setting for LoRA adaptors.

Comparison with Image-Diffusion Paradigm. To highlight the benefit of anchor-guided next-frame decoding with a VDM, we compare against a text-to-image (T2I) diffusion codec baseline that replaces our CogVideoX-5B decoder with Flux-dev-12B [107]. We fine-tune this larger model under three variants: (1) decode the bypass latent in a single step without the anchor branch; (2) concatenate the anchor latent along the channel dimension; (3) concatenate anchor latent as tokens (with 2D attention only, since 3D RoPE and attention is unsupported by IDM). As shown in Tab. 4, the BD-rate results indicate that the anchor condition is not effectively exploited in variants (1)–(3). Our method attains substantially lower BD-rates on LPIPS and DISTS, showing higher perceptual fidelity and better structural consistency with the source image.

We attribute these gains to the explicit anchor and virtual temporal evolution, which together enforce a strong latent–pixel dual-domain coupling. Concretely, the bypass latent provides a strong initialization in latent space, while the decoded anchor frame supplies a pixel-domain reference and leverages the VDM’s learned cross-frame consistency to mitigate semantic drift. These comparisons suggest that scaling parameters alone cannot achieve such impressive improvements. Additionally, what we propose is a **VDM-based paradigm**, which can benefit from future more efficient VDM backbones.

4.5 The Anchor and Bypass

We plot the rate-perceptual curves in Fig. 9 to compare the perceptual quality of the anchor and bypass frames (directly decoding bypass latent by Video-VAE) with the final reconstructed images. As shown, both the anchor and bypass frames exhibit lower perceptual quality, and the significant gap between their curves and the NeFIC curve highlights the effectiveness of our next-frame prediction strategy in achieving superior reconstruction fidelity with VDM.

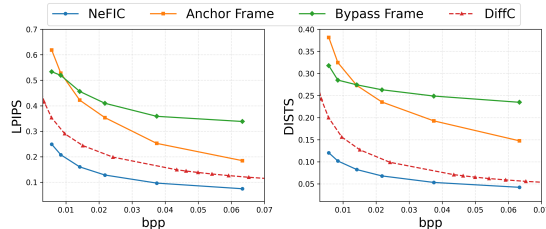


Figure 9: Comparisons of different frames.

5 Conclusion

We recast ultra-low-bitrate image compression as a virtual temporal evolution from a compact anchor frame to the final, fine-grained reconstruction. We introduce a generative next-frame decoder that leverages pretrained video diffusion priors to synthesize faithful, realistic images. To enable efficient generative decoding, we propose a two-stage training scheme: first, we adapt the VDM’s multi-frame generation to a next-frame prediction task tailored for image compression; second, we collapse the multi-step diffusion process into single-step generation. Our ULB-IC model NeFIC achieves superior perceptual compression performance with efficient decoding.

References

- [1] Johannes Ballé, Valero Laparra, and Eero P. Simoncelli. End-to-end optimized image compression. In *International Conference on Learning Representations*, 2017.
- [2] Johannes Ballé, David Minnen, Saurabh Singh, Sung Jin Hwang, and Nick Johnston. Variational image compression with a scale hyperprior. In *International Conference on Learning Representations*, 2018.
- [3] David Minnen, Johannes Ballé, and George D Toderici. Joint autoregressive and hierarchical priors for learned image compression. *Advances in neural information processing systems*, 31, 2018.
- [4] Dailan He, Ziming Yang, Weikun Peng, Rui Ma, Hongwei Qin, and Yan Wang. Elic: Efficient learned image compression with unevenly grouped space-channel contextual adaptive coding. In *Proceedings of the IEEE/CVF Conference on Computer Vision and Pattern Recognition*, pages 5718–5727, 2022.
- [5] Siqi Wu, Yinda Chen, Dong Liu, and Zhihai He. Conditional latent coding with learnable synthesized reference for deep image compression. In *Proceedings of the AAAI Conference on Artificial Intelligence*, volume 39, pages 12863–12871, 2025.
- [6] Renjie Zou, Chunfeng Song, and Zhaoxiang Zhang. The devil is in the details: Window-based attention for image compression. In *Proceedings of the IEEE/CVF conference on computer vision and pattern recognition*, pages 17492–17501, 2022.
- [7] Yinhao Zhu, Yang Yang, and Taco Cohen. Transformer-based transform coding. In *International Conference on Learning Representations*, 2022.
- [8] Jinming Liu, Heming Sun, and Jiro Katto. Learned image compression with mixed transformer-cnn architectures. In *Proceedings of the IEEE/CVF conference on computer vision and pattern recognition*, pages 14388–14397, 2023.
- [9] Yunuo Chen, Qian Li, Bing He, Donghui Feng, Ronghua Wu, Qi Wang, Li Song, Guo Lu, and Wenjun Zhang. S2cformer: Reorienting learned image compression from spatial interaction to channel aggregation, 2025.
- [10] Shiyu Qin, Jinpeng Wang, Yimin Zhou, Bin Chen, Tianci Luo, Baoyi An, Tao Dai, Shutao Xia, and Yaowei Wang. Mambavc: Learned visual compression with selective state spaces. *arXiv preprint arXiv:2405.15413*, 2024.
- [11] Yunuo Chen, Zezheng Lyu, Bing He, Hongwei Hu, Qi Wang, Yuan Tian, Li Song, Wenjun Zhang, and Guo Lu. Content-aware mamba for learned image compression. In *The Fourteenth International Conference on Learning Representations*, 2026.
- [12] Han Li, Shaohui Li, Wenrui Dai, Chenglin Li, Junni Zou, and Hongkai Xiong. Frequency-aware transformer for learned image compression. In *The Twelfth International Conference on Learning Representations*, 2024.
- [13] Fanhu Zeng, Hao Tang, Yihua Shao, Siyu Chen, Ling Shao, and Yan Wang. Mambaic: State space models for high-performance learned image compression. *arXiv preprint arXiv:2503.12461*, 2025.

- [14] Yunuo Chen, Zezheng Lyu, Bing He, Ning Cao, Gang Chen, Guo Lu, and Wenjun Zhang. Knowledge distillation for learned image compression. In *Proceedings of the IEEE/CVF International Conference on Computer Vision*, pages 4996–5006, 2025.
- [15] Yuqi Li, Haotian Zhang, Li Li, Dong Liu, and Feng Wu. Scaling learned image compression models up to 1 billion. *arXiv preprint arXiv:2508.09075*, 2025.
- [16] Yiwei Zhang, Guo Lu, Yunuo Chen, Shen Wang, Yibo Shi, Jing Wang, and Li Song. Neural rate control for learned video compression. In *The Twelfth International Conference on Learning Representations*, 2023.
- [17] Yuqi Li, Haotian Zhang, Li Li, and Dong Liu. Learned image compression with hierarchical progressive context modeling. *arXiv preprint arXiv:2507.19125*, 2025.
- [18] Jingbo Lu, Leheng Zhang, Xingyu Zhou, Mu Li, Wen Li, and Shuhang Gu. Learned image compression with dictionary-based entropy model. In *Proceedings of the Computer Vision and Pattern Recognition Conference*, pages 12850–12859, 2025.
- [19] Jiangchuan Li, Chuqin Zhou, Yunuo Chen, and Guo Lu. Differentiable vmf: A trainable metric for optimizing video compression codec. In *2025 IEEE International Symposium on Circuits and Systems (ISCAS)*, pages 1–5. IEEE, 2025.
- [20] Junhao Du, Chuqin Zhou, Ning Cao, Gang Chen, Yunuo Chen, Zhengxue Cheng, Li Song, Guo Lu, and Wenjun Zhang. Large language model for lossless image compression with visual prompts. *arXiv preprint arXiv:2502.16163*, 2025.
- [21] Ian Goodfellow, Jean Pouget-Abadie, Mehdi Mirza, Bing Xu, David Warde-Farley, Sherjil Ozair, Aaron Courville, and Yoshua Bengio. Generative adversarial networks. *Communications of the ACM*, 63(11):139–144, 2020.
- [22] Jiaming Song, Chenlin Meng, and Stefano Ermon. Denoising diffusion implicit models. *arXiv preprint arXiv:2010.02502*, 2020.
- [23] Jonathan Ho, Ajay Jain, and Pieter Abbeel. Denoising diffusion probabilistic models. *Advances in neural information processing systems*, 33:6840–6851, 2020.
- [24] Yiyang Ma, Wenhan Yang, and Jiaying Liu. Correcting diffusion-based perceptual image compression with privileged end-to-end decoder. *International conference on machine learning (ICML)*, 2024.
- [25] Marlene Careil, Matthew J Muckley, Jakob Verbeek, and Stéphane Lathuilière. Towards image compression with perfect realism at ultra-low bitrates. In *The Twelfth International Conference on Learning Representations*, 2024.
- [26] Zhiyuan Li, Yanhui Zhou, Hao Wei, Chenyang Ge, and Jingwen Jiang. Towards extreme image compression with latent feature guidance and diffusion prior. *IEEE Transactions on Circuits and Systems for Video Technology*, 2024.
- [27] Junyang Chen, Jinshan Pan, and Jiangxin Dong. Faithdiff: Unleashing diffusion priors for faithful image super-resolution. In *CVPR*, 2025.
- [28] Anle Ke, Xu Zhang, Tong Chen, Ming Lu, Chao Zhou, Jiawen Gu, and Zhan Ma. Ultra lowrate image compression with semantic residual coding and compression-aware diffusion. *arXiv preprint arXiv:2505.08281*, 2025.
- [29] Naifu Xue, Zhaoyang Jia, Jiahao Li, Bin Li, Yuan Zhang, and Yan Lu. Dlf: Extreme image compression with dual-generative latent fusion. *Proceedings of the IEEE/CVF International Conference on Computer Vision (ICCV)*, Oct 2025.
- [30] Zhengxue Cheng, Heming Sun, Masaru Takeuchi, and Jiro Katto. Learned image compression with discretized gaussian mixture likelihoods and attention modules. In *Proceedings of the IEEE/CVF conference on computer vision and pattern recognition*, pages 7939–7948, 2020.

- [31] Wei Jiang, Jiayu Yang, Yongqi Zhai, Peirong Ning, Feng Gao, and Ronggang Wang. Mlic: Multi-reference entropy model for learned image compression. In *Proceedings of the 31st ACM International Conference on Multimedia*, pages 7618–7627, 2023.
- [32] Wei Jiang and Ronggang Wang. MLIC++: Linear complexity multi-reference entropy modeling for learned image compression. In *ICML 2023 Workshop Neural Compression: From Information Theory to Applications*, 2023.
- [33] David Minnen and Saurabh Singh. Channel-wise autoregressive entropy models for learned image compression. In *2020 IEEE International Conference on Image Processing (ICIP)*, pages 3339–3343. IEEE, 2020.
- [34] MingSheng Zhou and MingMing Kong. Glic: General format learned image compression. In *Proceedings of the AAAI Conference on Artificial Intelligence*, volume 39, pages 10815–10824, 2025.
- [35] Shoma Iwai, Tomo Miyazaki, Yoshihiro Sugaya, and Shinichiro Omachi. Fidelity-controllable extreme image compression with generative adversarial networks. In *2020 25th International Conference on Pattern Recognition (ICPR)*, pages 8235–8242. IEEE, 2021.
- [36] Guo-Hua Wang, Jiahao Li, Bin Li, and Yan Lu. Evc: Towards real-time neural image compression with mask decay. *arXiv preprint arXiv:2302.05071*, 2023.
- [37] Eirikur Agustsson et al. Generative adversarial networks for extreme learned image compression. In *Proceedings of the IEEE/CVF International Conference on Computer Vision (ICCV)*, 2019.
- [38] Fabian Mentzer, George D Toderici, Michael Tschannen, and Eirikur Agustsson. High-fidelity generative image compression. *Advances in neural information processing systems*, 33:11913–11924, 2020.
- [39] Eirikur Agustsson, David Minnen, George Toderici, and Fabian Mentzer. Multi-realism image compression with a conditional generator. In *Proceedings of the IEEE/CVF Conference on Computer Vision and Pattern Recognition*, pages 22324–22333, 2023.
- [40] Matthew J Muckley, Alaaeldin El-Nouby, Karen Ullrich, Hervé Jégou, and Jakob Verbeek. Improving statistical fidelity for neural image compression with implicit local likelihood models. In *International Conference on Machine Learning*, pages 25426–25443. PMLR, 2023.
- [41] Nikolai Körber, Eduard Kromer, Andreas Siebert, Sascha Hauke, Daniel Mueller-Gritschneider, and Björn Schuller. Egic: enhanced low-bit-rate generative image compression guided by semantic segmentation. In *European Conference on Computer Vision*, pages 202–220. Springer, 2024.
- [42] Qi Mao, Tinghan Yang, Yinuo Zhang, Zijian Wang, Meng Wang, Shiqi Wang, Libiao Jin, and Siwei Ma. Extreme image compression using fine-tuned vqgans. In *2024 Data Compression Conference (DCC)*, pages 203–212. IEEE, 2024.
- [43] Naifu Xue, Qi Mao, Zijian Wang, Yuan Zhang, and Siwei Ma. Unifying generation and compression: Ultra-low bitrate image coding via multi-stage transformer. In *2024 IEEE International Conference on Multimedia and Expo (ICME)*, pages 1–6. IEEE, 2024.
- [44] Zhaoyang Jia, Jiahao Li, Bin Li, Houqiang Li, and Yan Lu. Generative latent coding for ultra-low bitrate image compression. In *Proceedings of the IEEE/CVF Conference on Computer Vision and Pattern Recognition*, pages 26088–26098, 2024.
- [45] Hageyoung Lee, Minkyu Kim, Jun-Hyuk Kim, Seungeon Kim, Dokwan Oh, and Jaeho Lee. Neural image compression with text-guided encoding for both pixel-level and perceptual fidelity. *arXiv preprint arXiv:2403.02944*, 2024.
- [46] Eric Lei, Yiğit Berkay Uslu, Hamed Hassani, and Shirin Saeedi Bidokhti. Text+ sketch: Image compression at ultra low rates. *arXiv preprint arXiv:2307.01944*, 2023.

- [47] Nikolai Körber, Eduard Kromer, Andreas Siebert, Sascha Hauke, Daniel Mueller-Gritschneider, and Björn Schuller. Perco (sd): Open perceptual compression. *arXiv preprint arXiv:2409.20255*, 2024.
- [48] Lucas Theis, Tim Salimans, Matthew D Hoffman, and Fabian Mentzer. Lossy compression with gaussian diffusion. *arXiv preprint arXiv:2206.08889*, 2022.
- [49] Alaaeldin El-Nouby, Matthew J Muckley, Karen Ullrich, Ivan Laptev, Jakob Verbeek, and Hervé Jégou. Image compression with product quantized masked image modeling. *arXiv preprint arXiv:2212.07372*, 2022.
- [50] Luoxu Jin and Hiroshi Watanabe. Perceptual image compression via stable diffusion at low bitrate. In *2024 IEEE 7th International Conference on Multimedia Information Processing and Retrieval (MIPR)*, pages 626–629. IEEE, 2024.
- [51] Xiaoyue Ling, Chuqin Zhou, Chunyi Li, Yunuo Chen, Yuan Tian, Guo Lu, and Wenjun Zhang. Free-gvc: Towards training-free extreme generative video compression with temporal coherence. *arXiv preprint arXiv:2602.09868*, 2026.
- [52] Tongda Xu, Ziran Zhu, Dailan He, Yanghao Li, Lina Guo, Yuanyuan Wang, Zhe Wang, Hongwei Qin, Yan Wang, Jingjing Liu, and Ya-Qin Zhang. Idempotence and perceptual image compression. In *The Twelfth International Conference on Learning Representations*, 2024.
- [53] Ruihan Yang and Stephan Mandt. Lossy image compression with conditional diffusion models. *Advances in Neural Information Processing Systems*, 36:64971–64995, 2023.
- [54] Lucas Relic, Roberto Azevedo, Markus Gross, and Christopher Schroers. Lossy image compression with foundation diffusion models. In *European Conference on Computer Vision*, pages 303–319. Springer, 2024.
- [55] Naifu Xue, Zhaoyang Jia, Jiahao Li, Bin Li, Yuan Zhang, and Yan Lu. One-step diffusion-based image compression with semantic distillation. *Advances in Neural Information Processing Systems*, 2025.
- [56] Juan Song, Lijie Yang, and Mingtao Feng. Extremely low-bitrate image compression semantically disentangled by Imms from a human perception perspective. *arXiv preprint arXiv:2503.00399*, 2025.
- [57] Chuqin Zhou, Xiaoyue Ling, Yunuo Chen, Jincheng Dai, Guo Lu, and Wenjun Zhang. Dual-representation image compression at ultra-low bitrates via explicit semantics and implicit textures. *arXiv preprint arXiv:2602.05213*, 2026.
- [58] Zhiyuan Li, Yanhui Zhou, Hao Wei, Chenyang Ge, and Ajmal Saeed Mian. Diffusion-based extreme image compression with compressed feature initialization. 2024.
- [59] Jianhui Chang. Generative image coding with diffusion prior. *arXiv preprint arXiv:2509.13768*, 2025.
- [60] Lei Lu, Yanyue Xie, Wei Jiang, Wei Wang, Xue Lin, and Yanzhi Wang. Hybridflow: Infusing continuity into masked codebook for extreme low-bitrate image compression. In *Proceedings of the 32nd ACM International Conference on Multimedia*, pages 3010–3018, 2024.
- [61] Tongda Xu, Jiahao Li, Bin Li, Yan Wang, Ya-Qin Zhang, and Yan Lu. Picd: Versatile perceptual image compression with diffusion rendering. In *Proceedings of the Computer Vision and Pattern Recognition Conference*, pages 28436–28445, 2025.
- [62] Jinpei Guo, Yifei Ji, Zheng Chen, Kai Liu, Min Liu, Wang Rao, Wenbo Li, Yong Guo, and Yulun Zhang. Oscar: One-step diffusion codec across multiple bit-rates. *arXiv preprint arXiv:2505.16091*, 2025.
- [63] Yichong Xia, Yimin Zhou, Jinpeng Wang, Baoyi An, Haoqian Wang, Yaowei Wang, and Bin Chen. Diffpc: Diffusion-based high perceptual fidelity image compression with semantic refinement. In *The Thirteenth International Conference on Learning Representations*, 2025.

- [64] Guo Lu, Jing Wang, Yunuo Chen, Chuqin Zhou, Yibo Shi, and Kai Lin. Vcip 2025 ultra low-bitrate video compression challenge. In *2025 International Conference on Visual Communications and Image Processing (VCIP)*, pages 1–3. IEEE, 2025.
- [65] Lvmin Zhang, Anyi Rao, and Maneesh Agrawala. Adding conditional control to text-to-image diffusion models. In *Proceedings of the IEEE/CVF international conference on computer vision*, pages 3836–3847, 2023.
- [66] Chong Mou, Xintao Wang, Liangbin Xie, Yanze Wu, Jian Zhang, Zhongang Qi, and Ying Shan. T2i-adapter: Learning adapters to dig out more controllable ability for text-to-image diffusion models. In *Proceedings of the AAAI conference on artificial intelligence*, volume 38, pages 4296–4304, 2024.
- [67] Denis Zavadski, Johann-Friedrich Feiden, and Carsten Rother. Controlnet-xs: Rethinking the control of text-to-image diffusion models as feedback-control systems. In *European Conference on Computer Vision*, pages 343–362. Springer, 2024.
- [68] Robin Rombach, Andreas Blattmann, Dominik Lorenz, Patrick Esser, and Björn Ommer. High-resolution image synthesis with latent diffusion models. In *Proceedings of the IEEE/CVF conference on computer vision and pattern recognition*, pages 10684–10695, 2022.
- [69] Jeremy Vonderfecht and Feng Liu. Lossy compression with pretrained diffusion models. *International Conference on Learning Representations*, 2025.
- [70] Noor Fathima Ghouse, Jens Petersen, Auke Wiggers, Tianlin Xu, and Guillaume Sautiere. A residual diffusion model for high perceptual quality codec augmentation. *arXiv preprint arXiv:2301.05489*, 2023.
- [71] Noor Fathima Khanum Mohamed Ghouse, Jens Petersen, Auke J Wiggers, Tianlin Xu, and Guillaume Sautiere. Neural image compression with a diffusion-based decoder. 2023.
- [72] Emiel Hoogeboom, Eirikur Agustsson, Fabian Mentzer, Luca Versari, George Toderici, and Lucas Theis. High-fidelity image compression with score-based generative models. *arXiv preprint arXiv:2305.18231*, 2023.
- [73] Wenyi Hong, Ming Ding, Wendi Zheng, Xinghan Liu, and Jie Tang. Cogvideo: Large-scale pretraining for text-to-video generation via transformers. *arXiv preprint arXiv:2205.15868*, 2022.
- [74] Ruben Villegas, Mohammad Babaeizadeh, Pieter-Jan Kindermans, Hernan Moraldo, Han Zhang, Mohammad Taghi Saffar, Santiago Castro, Julius Kunze, and Dumitru Erhan. Phenaki: Variable length video generation from open domain textual description. *arXiv preprint arXiv:2210.02399*, 2022.
- [75] Andreas Blattmann, Robin Rombach, Huan Ling, Tim Dockhorn, Seung Wook Kim, Sanja Fidler, and Karsten Kreis. Align your latents: High-resolution video synthesis with latent diffusion models. In *Proceedings of the IEEE/CVF conference on computer vision and pattern recognition*, pages 22563–22575, 2023.
- [76] Yuwei Guo, Ceyuan Yang, Anyi Rao, Zhengyang Liang, Yaohui Wang, Yu Qiao, Maneesh Agrawala, Dahua Lin, and Bo Dai. Animatediff: Animate your personalized text-to-image diffusion models without specific tuning. *arXiv preprint arXiv:2307.04725*, 2023.
- [77] Jonathan Ho, Tim Salimans, Alexey Gritsenko, William Chan, Mohammad Norouzi, and David J Fleet. Video diffusion models. *Advances in neural information processing systems*, 35:8633–8646, 2022.
- [78] Muyang Li, Ji Lin, Chenlin Meng, Stefano Ermon, Song Han, and Jun-Yan Zhu. Efficient spatially sparse inference for conditional gans and diffusion models. *Advances in neural information processing systems*, 35:28858–28873, 2022.
- [79] Uriel Singer, Adam Polyak, Thomas Hayes, Xi Yin, Jie An, Songyang Zhang, Qiyuan Hu, Harry Yang, Oron Ashual, Oran Gafni, et al. Make-a-video: Text-to-video generation without text-video data. *arXiv preprint arXiv:2209.14792*, 2022.

- [80] Hongjie Wang, Chih-Yao Ma, Yen-Cheng Liu, Ji Hou, Tao Xu, Jialiang Wang, Felix Juefei-Xu, Yaqiao Luo, Peizhao Zhang, Tingbo Hou, et al. Lingen: Towards high-resolution minute-length text-to-video generation with linear computational complexity. In *Proceedings of the Computer Vision and Pattern Recognition Conference*, pages 2578–2588, 2025.
- [81] Zhuoyi Yang, Jiayan Teng, Wendi Zheng, Ming Ding, Shiyu Huang, Jiazheng Xu, Yuanming Yang, Wenyi Hong, Xiaohan Zhang, Guanyu Feng, et al. Cogvideox: Text-to-video diffusion models with an expert transformer. *arXiv preprint arXiv:2408.06072*, 2024.
- [82] OpenAI. Sora, March 2024.
- [83] Team Wan, Ang Wang, Baole Ai, Bin Wen, Chaojie Mao, Chen-Wei Xie, Di Chen, Feiwu Yu, Haiming Zhao, Jianxiao Yang, et al. Wan: Open and advanced large-scale video generative models. *arXiv preprint arXiv:2503.20314*, 2025.
- [84] Weijie Kong, Qi Tian, Zijian Zhang, Rox Min, Zuozhuo Dai, Jin Zhou, Jiangfeng Xiong, Xin Li, Bo Wu, Jianwei Zhang, et al. Hunyuanvideo: A systematic framework for large video generative models. *arXiv preprint arXiv:2412.03603*, 2024.
- [85] OpenAI. Sora 2, March 2025.
- [86] Colin Raffel, Noam Shazeer, Adam Roberts, Katherine Lee, Sharan Narang, Michael Matena, Yanqi Zhou, Wei Li, and Peter J Liu. Exploring the limits of transfer learning with a unified text-to-text transformer. *Journal of machine learning research*, 21(140):1–67, 2020.
- [87] William Peebles and Saining Xie. Scalable diffusion models with transformers. In *Proceedings of the IEEE/CVF international conference on computer vision*, pages 4195–4205, 2023.
- [88] Jianlin Su, Murtadha Ahmed, Yu Lu, Shengfeng Pan, Wen Bo, and Yunfeng Liu. Roformer: Enhanced transformer with rotary position embedding. *Neurocomputing*, 568:127063, 2024.
- [89] Yijing Lin, Mengqi Huang, Shuhan Zhuang, and Zhendong Mao. Realgeneral: Unifying visual generation via temporal in-context learning with video models. *International conference on Computer Vision (ICCV)*, 2025.
- [90] Xi Chen, Zhifei Zhang, He Zhang, Yuqian Zhou, Soo Ye Kim, Qing Liu, Yijun Li, Jianming Zhang, Nanxuan Zhao, Yilin Wang, et al. Unireal: Universal image generation and editing via learning real-world dynamics. In *Proceedings of the Computer Vision and Pattern Recognition Conference*, pages 12501–12511, 2025.
- [91] Edward J Hu, Yelong Shen, Phillip Wallis, Zeyuan Allen-Zhu, Yuanzhi Li, Shean Wang, Lu Wang, Weizhu Chen, et al. Lora: Low-rank adaptation of large language models. *ICLR*, 1(2):3, 2022.
- [92] Tim Salimans and Jonathan Ho. Progressive distillation for fast sampling of diffusion models. *arXiv preprint arXiv:2202.00512*, 2022.
- [93] Richard Zhang, Phillip Isola, Alexei A Efros, Eli Shechtman, and Oliver Wang. The unreasonable effectiveness of deep features as a perceptual metric. In *Proceedings of the IEEE conference on computer vision and pattern recognition*, pages 586–595, 2018.
- [94] Tianyu Zhang, Xin Luo, Li Li, and Dong Liu. Stablecodec: Taming one-step diffusion for extreme image compression. *arXiv preprint arXiv:2506.21977*, 2025.
- [95] Jiahao Li, Bin Li, and Yan Lu. Hybrid spatial-temporal entropy modelling for neural video compression. In *Proceedings of the 30th ACM International Conference on Multimedia*, pages 1503–1511, 2022.
- [96] Jiahao Li, Bin Li, and Yan Lu. Neural video compression with diverse contexts. In *Proceedings of the IEEE/CVF Conference on Computer Vision and Pattern Recognition*, pages 22616–22626, 2023.

- [97] Alec Radford, Jong Wook Kim, Chris Hallacy, Aditya Ramesh, Gabriel Goh, Sandhini Agarwal, Girish Sastry, Amanda Askell, Pamela Mishkin, Jack Clark, et al. Learning transferable visual models from natural language supervision. In *International conference on machine learning*, pages 8748–8763. PmLR, 2021.
- [98] Nupur Kumari, Richard Zhang, Eli Shechtman, and Jun-Yan Zhu. Ensembling off-the-shelf models for gan training. In *Proceedings of the IEEE/CVF conference on computer vision and pattern recognition*, pages 10651–10662, 2022.
- [99] Jiaheng Liu, Guo Lu, Zhihao Hu, and Dong Xu. A unified end-to-end framework for efficient deep image compression. *arXiv preprint arXiv:2002.03370*, 2020.
- [100] Eastman Kodak. Kodak lossless true color image suite (photocd pcd0992), 1993. Available from <http://r0k.us/graphics/kodak/>.
- [101] George Toderici, Wenzhe Shi, Radu Timofte, Lucas Theis, Johannes Balle, Eirikur Agustsson, Nick Johnston, and Fabian Mentzer. Workshop and challenge on learned image compression (clic2020), 2020.
- [102] Eirikur Agustsson and Radu Timofte. Ntire 2017 challenge on single image super-resolution: Dataset and study. In *Proceedings of the IEEE conference on computer vision and pattern recognition workshops*, pages 126–135, 2017.
- [103] Keyan Ding, Kede Ma, Shiqi Wang, and Eero P Simoncelli. Image quality assessment: Unifying structure and texture similarity. *IEEE transactions on pattern analysis and machine intelligence*, 44(5):2567–2581, 2020.
- [104] Martin Heusel, Hubert Ramsauer, Thomas Unterthiner, Bernhard Nessler, and Sepp Hochreiter. Gans trained by a two time-scale update rule converge to a local nash equilibrium. *Advances in neural information processing systems*, 30, 2017.
- [105] Mikołaj Bińkowski, Danica J Sutherland, Michael Arbel, and Arthur Gretton. Demystifying mmd gans. *arXiv preprint arXiv:1801.01401*, 2018.
- [106] Gisle Bjontegaard. Calculation of average psnr differences between rd-curves. In *VCEG-M33*, 2001.
- [107] Black Forest Labs. Flux. <https://github.com/black-forest-labs/flux>, 2024.